Open-Circuit Fault-Tolerant Control and Topology Switching Strategy of Active Magnetic Bearing Power Electronics Controller

Jianfu Ding, *Student Member, IEEE*, Hongbo Sun, Dong Jiang, *Senior Member, IEEE*, Jichang Yang, and Zicheng Liu, *Member, IEEE*

***Abstract*—Active magnetic bearing (AMB) technology has been widely used in high-speed electrical machines. Power electronics controller amplifier is an important segment in AMB system. Failure of power electronics device is a common threat to the reliability of AMB amplifier and can cause serious damage. In order to improve the robustness of the amplifier, this article proposes open-circuit fault-tolerant control strategies based on different topologies. For single-axis systems, a pair of windings with a single degree of freedom can work in four different working modes based on the three-phase full-bridge structure. It can detect and locate the open-circuit fault of a power electronics switch in operation. After promotion to multiaxis systems, a novel kind of topology for amplifier with fault tolerant strategy has been proposed that can also detect the open-circuit fault of power electronics switch and switch to fault tolerance mode for a multiaxis system. Fault tolerant experiments verify the feasibility and rapid response of different fault tolerance strategies with an AMB testbed in this article.**

***Index Terms*—Active magnetic bearing (AMB), amplifier, open-circuit fault-tolerant control, topology switching.**

I. Introduction

Active magnetic bearing (AMB) is a novel kind of supporting device for rotational machinery. AMB levitates the rotor without physical contact and it can provide active magnetic force. It has almost no mechanical loss except for windage, suspending the rotor to reach a high operating speed. It has the characteristics of low maintenance and lubrication requirement, so AMB has been widely applied in high-speed (HS) motor, flywheel energy storage, artificial heart pump [1]–[3]. In recent years, in-depth research has been conducted in the field of AMB and product development, and the development of electromagnetic bearings still has broad prospects in the next few decades [4]. With the gradual increase in the rotational speed of the rotating machines applied to AMBs, the requirements for safety and reliability of AMB system also gradually increase. Commonly used security designs reduce the risk of system failure and improve the security of the system by taking measures, such as system programs, software development tools, and redundant components [5]. Yu and Zhu [6] proposed a fault-tolerant strategy proposed for sensors.

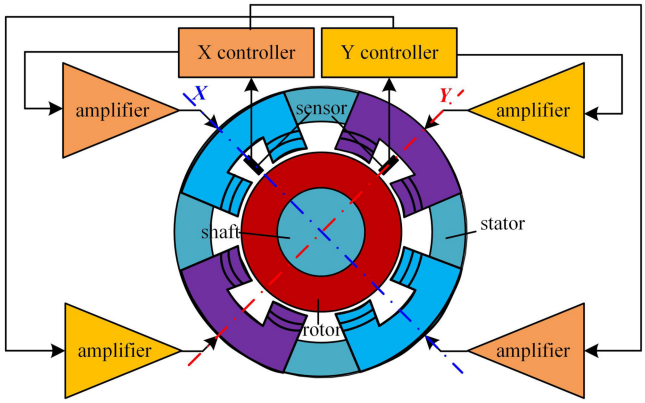

Fig. 1. Structure of radial AMB control system.

AMB system is a control system, generally includes displacement sensors, displacement controller, amplifier, etc. The structure of the AMB system is shown in Fig. 1 for a two-axis plane. The sensors detect the displacement of rotor in *X*- and *Y*-directions, and feed them back to the controller, and the controller generates the command value of each winding current and transmits it to the amplifier. The amplifier converts the control signal into the winding current to control the electromagnetic force on the bearing and then controls the bearing position to make it stably suspended.

For AMB system, amplifier is an important segment to generate control current and magnetic force. There are two kinds of power amplifiers—the linear power amplifier and the switching power amplifier. The linear power is composed by analog circuit, because of low efficiency and serious heat, it is replaced by

Manuscript received October 29, 2021; revised February 16, 2022; accepted March 10, 2022. Date of publication March 17, 2022; date of current version May 23, 2022. This work was supported in part by the sponsorship of the National Natural Science Foundation of China (NSFC) under Grant 51877091. Recommended for publication by Associate Editor Y. A.-R. I. Mohamed. *(Corresponding author: Dong Jiang.)*

Jianfu Ding is with the State Key Laboratory of Advanced Electromagnetic Engineering and Technology, China-EU Institute for Clean and Renewable Energy, Huazhong University of Science and Technology, Wuhan 430074, China (e-mail: djf@hust.edu.cn).

Hongbo Sun is with the China Ship Development and Design Center, Wuhan 430064, China (e-mail: sun919327232@126.com).

Dong Jiang, Jichang Yang, and Zicheng Liu are with the State Key Laboratory of Advanced Electromagnetic Engineering and Technology, School of Electrical and Electronic Engineering, Huazhong University of Science and Technology, Wuhan 430074, China (e-mail: jiangd@hust.edu.cn; yangjc@hust.edu.cn; liuzc@hust.edu.cn).

Color versions of one or more figures in this article are available at https://doi.org/10.1109/TPEL.2022.3159959.

Digital Object Identifier 10.1109/TPEL.2022.3159959

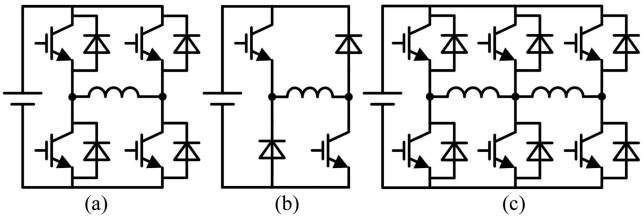

Fig. 2. AMB drive topologies. (a) Full H-bridge. (b) Half H-bridge. (c) Shared-leg full bridge.

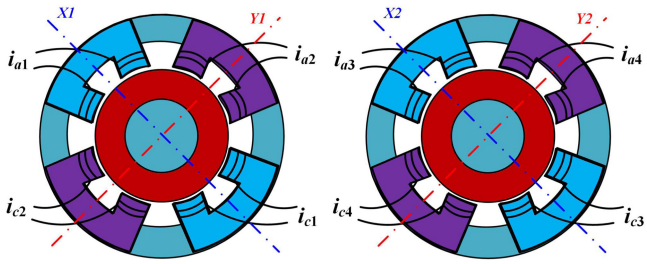

Fig. 3. Arrangement of coils in AMBs.

power electronic circuit gradually. Switching power amplifier, with high efficiency and good dynamic characteristic, is widely used now [7], [8].

Generally, the amplifier is a current control system. As a result, for the whole system, the outer control loop is the displacement control loop and the inner control loop is the current loop. The inner loop current loop usually uses a proportional integral (PI) controller. The most basic control method of the position loop is a proportional derivative (PD) controller. In order to eliminate static errors, a PI derivative (PID) controller can be used. Because the PID controller is easy to realize and with effectiveness, it is usually used for engineering control [9]. In addition, in order to reduce the fluctuation of the rotor displacement, many control methods of vibration suppressing have been proposed [10], [11]. He *et al.* [12] presents an improved current control strategy. Noshadi *et al.* [13] studies the identification and robust control of a multi-input multioutput AMB system. All control strategies and research are to improve the robustness and stability of the active magnetic levitation system.

For AMB power electronics controller, full-bridge topology is the first switching type electronic converter used in an AMB system. It can be able to control the current in two directions. Since the winding current in AMB varies near the bias current with control current, the current is unidirectional. Half of the devices in Fig. 2(a) can be saved and it is still able to control unidirectional winding current, as shown in Fig. 2(b). This topology can be called half H-bridge converter. Since each axis of AMB is with two windings and their reference currents are related to each other, the topology of currents together, called shared-leg full bridge converter, as shown in Fig. 2(c). It is a three-phase voltage source converter in fact. The two windings share the central phase-leg and the current can be controlled through the switching of the two phase-leg in the two sides [14]. For a multiaxis system, the AMB drive has been proposed in [15].

In power electronic circuits, open-circuit fault of switching devices is a common malfunction. The major failure mode is because of the fatigue of device wire-bonding in the thermal cycle of operation, as well as the failure of the gate driver. This kind of failure mode behaves like switch open-circuit in its conduction direction, but will not impact the antiparalleled diode, bringing an opportunity for fault-tolerant control [15].

Many scholars have studied the method of magnetic bearing fault detection. Cheng *et al.* [16] provides a fault-diagnosis method based on the equivalent slope of current. Yang *et al.* [17] provides a series-winding topology converter for fault-tolerant operation. Switching device failures in power electronic circuits also occur in other drive systems, and many fault-tolerant control strategies have been proposed [18]–[22], including switch reluctance motor drives [18], grid-connected neutral-point clamped inverter system [19], permanent-magnet synchronous motor drives [20], etc. All fault-tolerant control strategies are to diagnose fault types in time and keep the system running stably.

In the AMB system, if the open-circuit fault occurs, the rotor will drop and the system will be unstable, which can even cause a catastrophic accident. As a result, the amplifier is supposed to possess fault-tolerance ability, which is meaningful for the safety of AMB system.

Jiang *et al.* [15] introduced a fault-tolerant control method based on device open-circuit failure for single-axis AMB drive of three-phase-full-bridge converter[see Fig. 2(c)]. There are only two modes for the converter. For the normal and backup modes, the current stress in the central phase-leg is big. Based on the current direction independence for AMB force, there should be multiple modes for the AMB drive in Fig. 2(c) and some of them can obtain much less current stress based on current cancelation in the central phase-leg. The fault-tolerant control method cannot locate the failed device, either. Further, for multiaxis AMB drive, the central phase-leg can be shared by different axis and there will be more modes for fault-tolerant control.

This article proposes the fault-tolerant control strategies which are applied in amplifiers for AMB system. The single-axis control strategy is based on a three-phase full-bridge topology. It will be introduced in Section II. Extended to multiaxis fault-tolerant control strategy, which is a fault-tolerant mechanism of the entire system based on the multiaxis control topology. It will be introduced in Section III. In order to verify the feasibility and effectiveness of the fault-tolerant strategies, experiments were carried out on the magnetic suspension four-bearing platform. The experimental results of fault-tolerant control after man-made open-circuit faults are shown in Section IV. Finally, Section V concludes the article.

In this article, the analysis and experiments are based on a typical four-axis radial AMB system. The arrangement of windings of two magnetic bearings is shown in Fig. 3. Each axis is inclined at 45° to share the weight of shaft and provide electromagnetic force together [23].

II. Single Axis Fault-Tolerant

In AMB systems, power electronic devices are the most vulnerable part of system reliability, and device redundancy is usually adopted to improve system safety performance. By means of device redundancy, the topology selectivity of controlling the

winding current is improved. Also, because AMB is based on Maxwell force which is independent of current direction, the redundant devices can be used to levitate the target even with the reversed current. Therefore, after the power electronic device fails, the system can be quickly changed from the fault state to the stable operation state by switching the circuit topology. In this section, a single axis fault-tolerance strategy is introduced.

A. Power Electronics Failure in Magnetic Bearing Drive

The actual operation of the power electronic circuit of the AMB shows that most of the faults are the damage of the power switching device, that is, the failure of the switching tube. The open-circuit fault and short-circuit fault of the power switching device are the most common. Sudden change in winding current. Among them, a short-circuit fault will change the circuit structure and it is difficult to design a fault-tolerant control method. The right action is to block the system and shut down immediately.

The power switching device which is used in the power circuits discussed in this article is insulated gate bipolar transistor (IGBT). As mentioned in the introduction, the open-circuit failure is a very possible failure mode because of the fatigue of wire-bonding in the package. The original conduction path of the winding current is blocked, but unlike the short-circuit failure, leaving some space for fault-tolerant control. In the IGBT power module, the failure of IGBT and diode in each switching unit are in separate substrates, and it has not much influence on the antiparalleled diode. After an open-circuit failure occurs, the circuit can be switched to the redundant mode to quickly return to the normal operating mode according to the location of the failed device.

B. Fault-Tolerant Drive Architecture

The single axis AMB drive architecture is based on the three-phase full-bridge topology, which is a very common power electronics power stage in application. Under normal operating conditions, according to the reverse common bridge arm structure and the common bridge arm t-b-t and b-t-b structures [15], the three-phase full bridge topology can have four working modes. The main difference between the four working topologies is the direction of the winding current. In AMB which is based on Maxwell Force, the change of the winding current direction will not affect the electromagnetic force. When any switch device has an open-circuit fault, it can be switched to other working modes as needed to realize switch from the fault state to the normal state.

As it shown in Fig. 4, when the drive module works in mode a, *S*2, *S*3, and *S*6 are activated and the rest switching elements are blocked, it controls the two winding currents to flow from the middle bridge arm. While the drive module works in mode b, *S*1, *S*4, and *S*5 are activated and the rest switching elements are blocked, it can control the current in the "backward" direction compared with the mode a. When the drive module works in mode c, *S*2, *S*3, *S*4, and *S*5 are activated and the rest switching elements are blocked, one winding current flows out from the middle bridge arm, and the other winding current flows toward the middle bridge arm. While the drive module works in mode d, *S*1, *S*3, *S*4, and *S*6 are activated and the rest switching elements are blocked, it can control the current in the "backward" direction compared with the mode c.

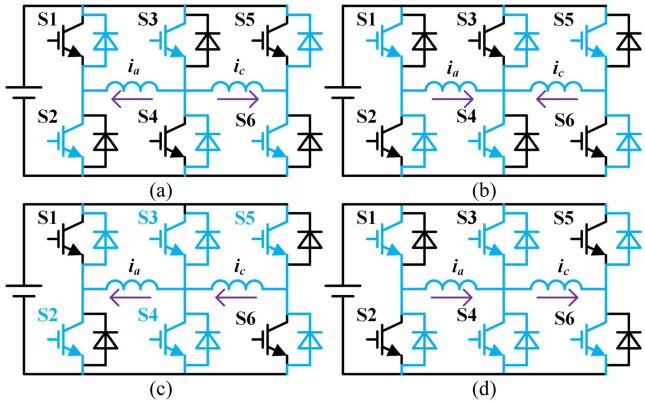

Fig. 4. Four working modes of three-phase full bridge in AMB system. (a) Mode a. (b) Mode b. (c) Mode c. (d) Mode d.

C. Fault-Tolerant Control and Implementation

The control block diagram of this fault-tolerant strategy is shown in Fig. 5. The current controller is in normal mode during normal operation. When a fault signal is detected, the current controller is switched to fault-tolerant mode. After switching the topology, the current of one phase winding will be reversed, so the reference current command value will be reversed. The circuit controller outputs the new duty cycle signal to the pulsewidth modulation (PWM) module, and the winding current signal is sent to the fault detection module. After the topology and controller mode are switched, the system will return to a stable state.

According to the topology shown in Fig. 5, assuming that the s_{i} is the switch variable of leg $i(i = 1,2,3)$. When the switch device of leg is turned ON, then $s_i = 1$. When the switch device of leg i is turned OFF, then $s_i = 0$. The variable u_i is the voltage at the middle point of leg $i(i = 1,2,3)$. The U_D is the voltage of dc-link. The relationship between u_i and s_i is as show as the left formula of (1). In the case of the average model, the voltage is controlled by the duty cycle of each switch device. Variable $d_1 \sim d_3$ represent the duty cycle of the switch devices, then the voltage is represented as the right part of

$$\begin{bmatrix} u_1 \\ u_2 \\ u_3 \end{bmatrix} = \begin{bmatrix} s_1 \\ s_2 \\ s_3 \end{bmatrix} \times U_D \overset{\text{averaging}}{\Rightarrow} \begin{bmatrix} U_1 \\ U_2 \\ U_3 \end{bmatrix} = \begin{bmatrix} d_1 \\ d_2 \\ d_3 \end{bmatrix} \times U_D. \quad (1)$$

Variable i_a and i_c represent the current of the windings, and the corresponding relationships are shown in Fig. 5. Assuming that the impedance of each winding is Z, the winding current can be expressed as

$$i_a = (U_2 - U_1)/Z, i_c = (U_3 - U_2)/Z. \quad (2)$$

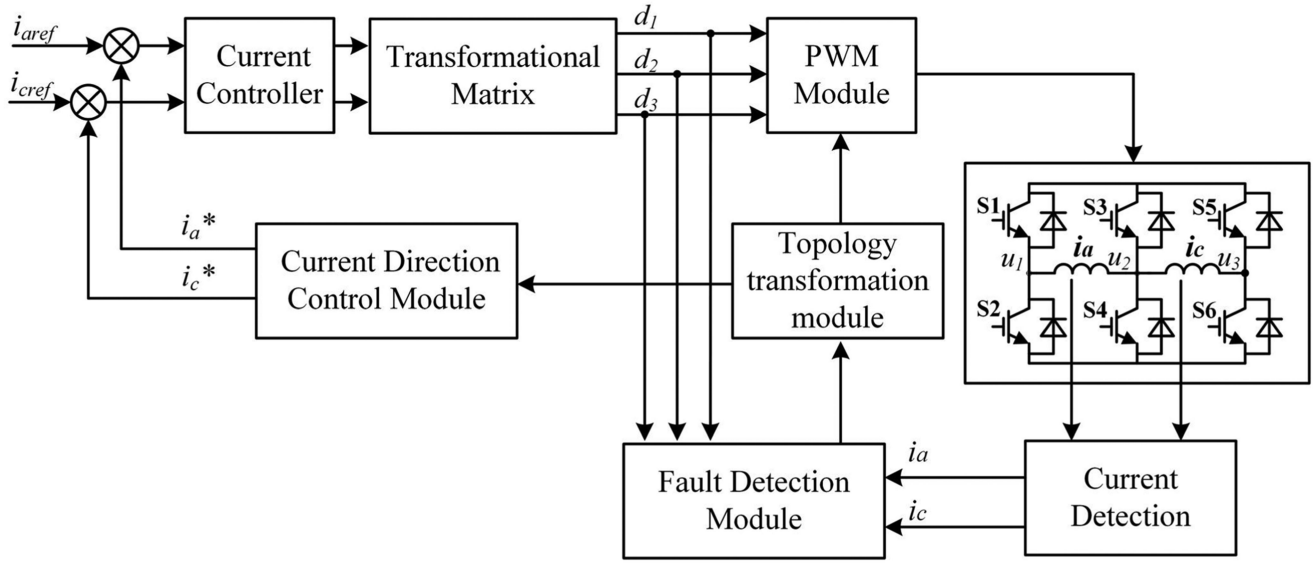

Fig. 5. The control block diagram of single axis fault-tolerant strategy.

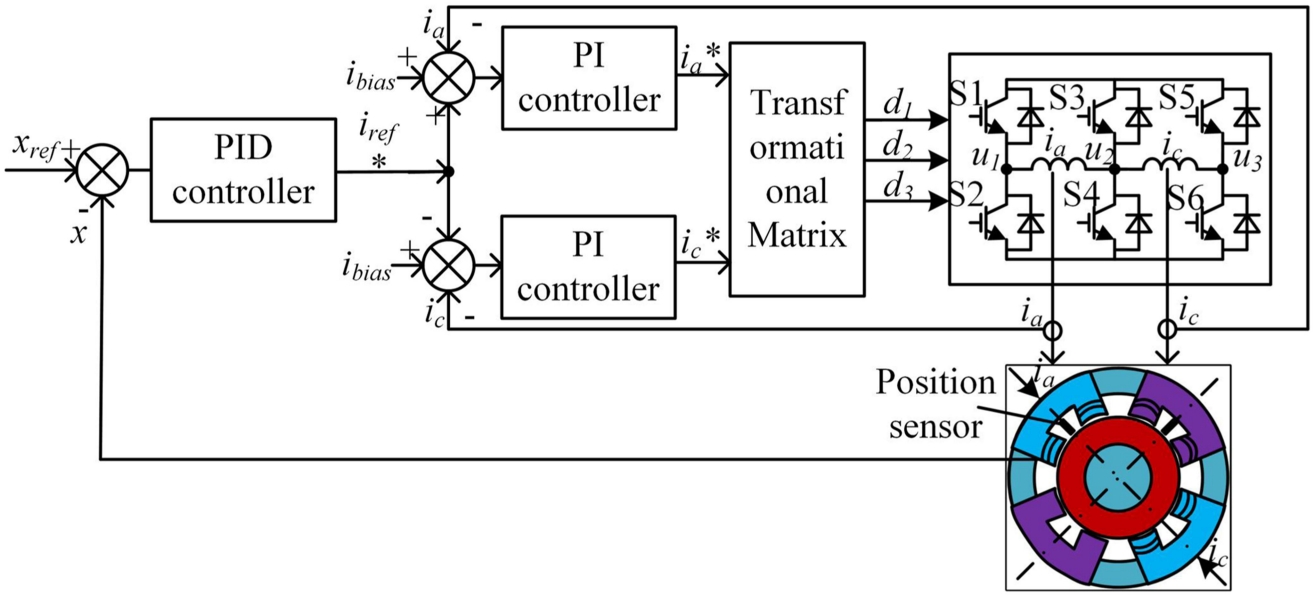

Fig. 6. Control block diagram of single-degree-of-freedom AMB.

The matrix expression of the voltages to the currents is expressed as

$$\begin{bmatrix} i_a \\ i_c \end{bmatrix} = \frac{1}{Z}\begin{bmatrix} -1 & 1 & 0 \\ 0 & -1 & 1 \end{bmatrix}\begin{bmatrix} U_1 \\ U_2 \\ U_3 \end{bmatrix}. \tag{3}$$

Then, we can define that the average value of the phase leg voltages is equals to $U_D/2$, making the voltage of each leg vary in the same range on both sides of the average value

$$\frac{1}{3}(U_1 + U_2 + U_3) = \frac{1}{2}U_D. \tag{4}$$

According to the formula (1), (3), and (4), we can get the PWM duty cycle transformation matrix T from the current command value to the PWM command value

$$\begin{bmatrix} i_a \\ i_c \\ U_D \end{bmatrix} = \frac{1}{Z}\begin{bmatrix} -1 & 1 & 0 \\ 0 & -1 & 0 \\ \frac{2}{3}Z & \frac{2}{3}Z & \frac{2}{3}Z \end{bmatrix}\begin{bmatrix} d_1 \\ d_2 \\ d_3 \end{bmatrix} \times U_D. \tag{5}$$

According to (5), combined with PI controller, the instruction value of the voltage of each phase leg can be obtained according to the reference current value. The single-degree-of-freedom AMB control block diagram is shown in in Fig. 6. In the current control loop, one degree of freedom and two winding currents decouple each other. In the case of i_a^*, the block diagram of the i_a control is simplified and shown in Fig. 7. Setting the PI parameters as: $k_p = \omega_c L/U_D$; $k_i = \omega_c R/U_D$; ω_c is the bandwidth of the current loop; L is the winding inductance; and R is the

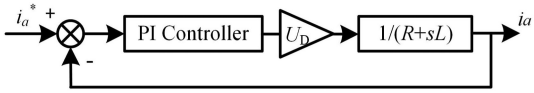

Fig. 7. Block diagram of i_a control.

winding resistance. The open-loop transfer function is expressed as

$$G(s) = \left(k_p + \frac{k_i}{s}\right)\left(\frac{U_D}{R + sL}\right) = \frac{\omega_c}{s}. \tag{6}$$

The bandwidth of the current loop can be changed by adjusting the PI parameters. The bandwidth of the current loop should be much larger than that of the position loop in actual design.

Jiang *et al.* [5] indicate the relationship between electromagnetic force and linearized force/current and force/displacement stiffness is

$$f(i, x) = k_i i - k_x x \tag{7}$$

where k_x is the force/displacement stiffness and k_i is the force/current stiffness. Refer to the general second-order spring system

$$m\ddot{x} + d\dot{x} + kx = 0 \tag{8}$$

where k is the linear stiffness coefficient, d is the damping coefficient, m is the mass, and x is the displacement. According to (7) and (8), the current value can be obtained

$$i(x) = -\frac{(k - k_x)x + d\dot{x}}{k_i}. \tag{9}$$

The PD parameters of position controller can be designed as follows:

$$\begin{cases} P = -\frac{k - k_x}{k_i} \\ D = -\frac{d}{k_i} \end{cases}. \tag{10}$$

By changing the control parameters of the system position loop, the stiffness and damping values of the system can be actively adjusted.

Compared with the control method where the duty ratio of the intermediate bridge arm is fixed [14], this method can determine the difference of the fault location according to the change of the duty ratio command values of the three bridge arms. The specific judgment method will be explained in the following section.

D. Fault Detection and Reaction

The reverse common-arm topology was initially adopted. After an open-circuit fault occurs, since the sum of the winding currents of one degree of freedom is twice the bias current, it can be judged whether the open-circuit fault has occurred by judging whether the sum of the winding currents is reduced. Here we set the current threshold I_{limit}. The bias current is I_{bias} under normal working conditions. Therefore, the sum of the two winding currents of a single degree of freedom is $2I_{\text{bias}}$. When it is detected that the sum of the two winding currents is less than the set current threshold, it is concluded that the switching device in the topology has an open-circuit fault. This is the first

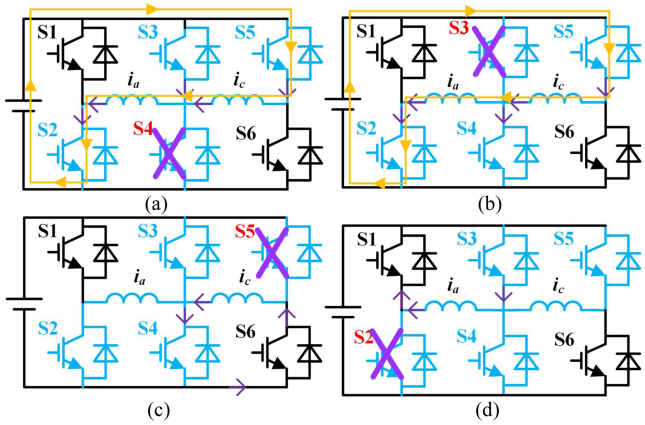

Fig. 8. Four fault-tolerant working modes of three-phase full bridge in AMB. (a) Fault mode a. (b) Fault mode b. (c) Fault mode c. (d) Fault mode d.

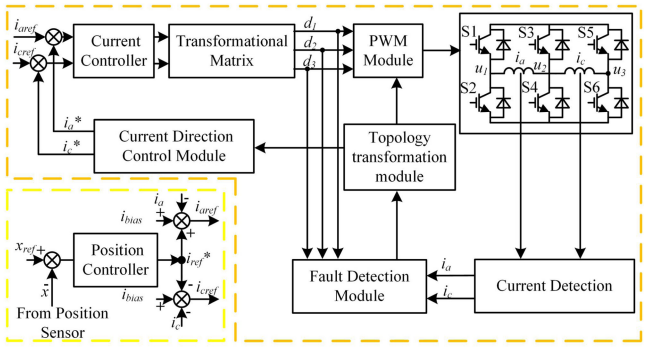

Fig. 9. Control block diagram of single axis AMB.

step. Then we have to determine which switching device has an open-circuit fault.

Here, we take Fig. 4(c) as an example. Under normal working conditions, the working topology is mode c shown in Fig. 4. When *S*2 or *S*5 has an open-circuit fault, the current of the corresponding winding i_a or i_c will decrease rapidly due to the lack of charging circuit, shown in Fig. 8(c) and (d). The corresponding bridge arm duty cycle command value will also change suddenly and reach the upper limit quickly. When the two middle bridge arm switching devices of *S*3 or *S*4 have an open-circuit fault, due to the limitation of the topology, in the case of fault in Fig. 8(a), the winding current $i_a \geq i_c$, in the case of fault in Fig. 8(b), the winding current $i_a \leq i_c$. If the winding current does not meet the limits of the above two fault topologies under normal control conditions, the command value of the duty cycle of each bridge arm will also change suddenly. The single degree of freedom control block diagram is shown in Fig. 9.

Specifically, when *S*2 has an open-circuit fault. First, the current i_a will drop sharply. Correspondingly, the duty cycle command value d_1 of the first bridge arm will drop sharply, and the duty cycle command value d_2 of the second bridge arm will rise sharply, that is, the midpoint voltage u_1 of the first bridge arm decreases, and the midpoint voltage u_2 of the second bridge arm will increase of the second bridge arm increasesw, modulating the current i_a in the increasing direction. Because of the sharp drop in current under this fault state, it can be

TABLE I
DUTY CYCLE CHANGES AND TOPOLOGY SWITCHING

Faulty device	d1	d2	d3	Mode switch
S2	0	1	1	c to d
S3	0	1	0	c to b
S4	1	0	1	c to a
S5	0	0	1	c to d

considered that the transient time is short, only the current loop works and the current reference value remains unchanged. After that, the current i_c feedback value does not change, and due to the increase of u_2, the current i_c has a downward trend. In order to keep the i_c current unchanged, the duty cycle command value d_3 of the third bridge arm will increase, that is, the midpoint voltage u_3 of the second bridge arm increases. When S5 has an open-circuit fault, it is similar to *S*2.

When *S*3 and *S*4 have an open-circuit fault, the situation is slightly different. Specifically, when *S*3 has an open-circuit fault. Since the normal charging loop of the winding i_a is disconnected, the current i_a will decrease, since there is still a charging loop which is shown in Fig. 8(b). The current i_a decreases slowly compared with the above situation, and the position loop will work at this time. After a fault occurs, rotor will drop and the position loop command value will increase because of the current aberrant. The i_a current will be adjusted in an increasing direction, and the i_c current will be adjusted in a decreasing direction. d_1 will increase and d_2 will decrease, that is, u_1 will decrease and u_2 will increase. In order to reduce the current i_c, d_3 will be reduced, that is, u_3 will be reduced. When *S*4 has an open-circuit fault, it is similar with *S*3.

The upper and lower thresholds of the duty cycle of the bridge arm are set to detect the device open-circuit fault. When the change of the duty cycle exceeds the upper threshold, it is recorded as 1, and when the duty cycle is lower than the lower threshold, it is recorded as 0. In this way, the transformation matrix and specific switching strategies can be obtained. As given in Table I. The mode switching strategy is shown in the last row. The corresponding mode is shown in Fig. 4.

This is the second step of the fault judgment strategy, which uses the change of the duty cycle command value of the bridge arm to locate the switching device that has an open-circuit fault, and finally performs topology switching according to the location of the fault.

The entire fault tolerance process is shown in Fig. 10.

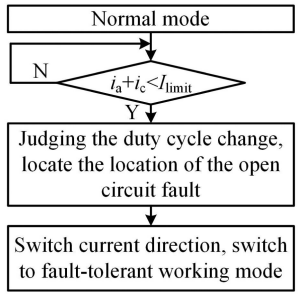

Fig. 10. Fault tolerance process.

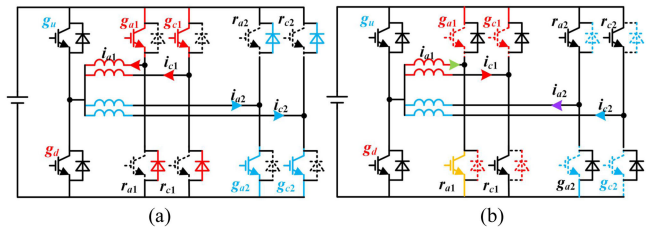

Fig. 11. Modes of amplifier. (a) Normal mode. (b) Auxiliary mode.

III. MULTIAXIS FAULT-TOLERANT

The fault-tolerant method introduced in Section II is for the power electronics controller in one-axis with two windings. The multiaxis fault-tolerant strategy is also the fault-tolerant strategy proposed by the multiaxis current control topology for the open-circuit fault of the switching device [15]. The different multiaxis control topologies are divided into normal and fault-tolerant operating modes. In this section, multiaxis fault-tolerant strategy is introduced.

A. Fault-Tolerant Drive Architecture and Control

As discussed in Section II, AMB is based on Maxwell force and is independent of winding current direction. With a shared-bridge converter for dual-axis AMB controller shown in Fig. 9, each winding is with bidirectional current control capability. In order to reduce the current stress in the common bridge, two windings are with "left side" current and the other two windings are with "right side" current in normal mode [see Fig. 11(a)].

Then, the current stress of shared phase-leg is expressed as

$$I_s = (i_{a1} + i_{c1}) - (i_{a2} + i_{c2}). \tag{11}$$

Considering the symmetry of the coils, $I_s \approx 0$

$$[i_{a1}\ i_{c1}] \approx [i_{a2}\ i_{c2}]. \tag{12}$$

The g_u, g_d, g_{ai}, g_{ci}, r_{ai}, $r_{ci}(i = 12)$ are PWM signals to drive the switching devices. The duty cycle of g_u and g_d are set as 0.5, but with opposite phases. The g_{ai} and g_{ci} are PWM signals applied in normal mode. When open-circuit occurs in switching device of certain phase-leg, transferring the switch device in this phase-leg and reversing its current will also keep the amplifier working. So certain signals of g_{ai} will be shielded and proper signals of r_{ci} will be applied to switch the mode.

For example, if the switch device becomes open-circuit in phase-leg i_{a1}, the spare switching device will be applied to reverse i_{a1} and i_{c1}, the amplifier works in auxiliary mode as Fig. 11(b). Obviously, there are many other kinds of auxiliary mode to tolerant when open-circuit fault occurs in other phase-legs for other DOF. The fault-tolerant topology of *N* degrees of freedom is shown in Fig. 12. In the normal mode, the noncommon bridge arm of each degree of freedom has two switching devices that can be open-circuit fault tolerant. Two switching devices with any one degree of freedom correspond to the same fault-tolerant working mode. For *N*-degree-of-freedom

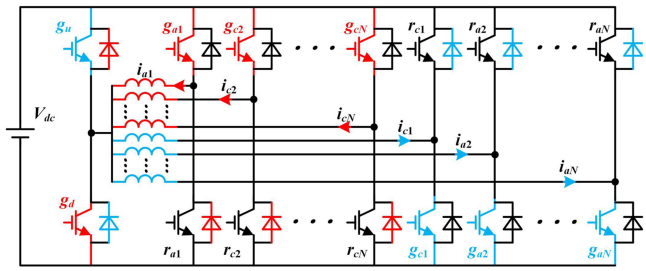

Fig. 12. *N*-degree-of-freedom fault-tolerant topology.

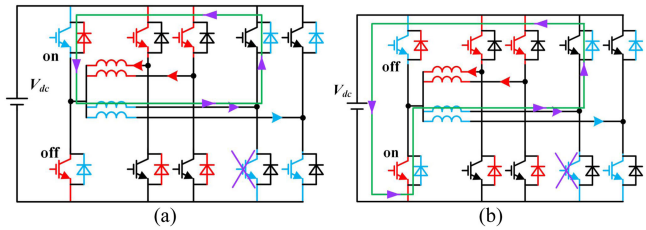

Fig. 13. Paths of current when fault occurs. (a) Path 1. (b) Path 2.

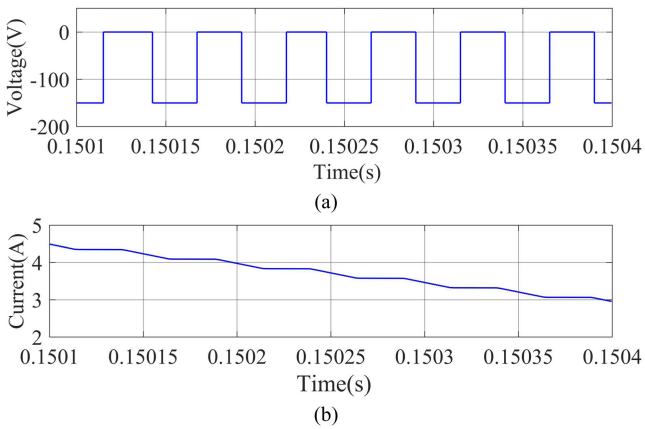

Fig. 14. Phenomenon when fault occurs. (a) Voltage of coil. (b) Current of coil.

topology, there are 2*N*+2 switching devices, corresponding to *N* kinds of fault-tolerant topologies.

B. Fault Analysis and Detection

Assuming the open-circuit fault occurs on the lower switch device of phase-leg i_{c1}. In one switching cycle, the path of current in the coil connected in this phase-leg is shown in Fig. 13. The dc-bus voltage $V_{\rm dc}$ is set as 150 V. When the current flows in path 1, the voltage of the coil is nearly zero, so the current declines little. When the current flows in path 2, the voltage of the coil is $-V_{\rm dc}$, so the current declines sharply. Because the duty cycle of shared-bridge is 0.5, every above path occupies half of the time in one switching cycle. As a result, declining of current in coil can be applied to detect the open-circuit fault. The voltage and current of the coil when an open-circuit occurs are shown in Fig. 14.

Based on the analysis above, when an open-circuit fault occurs, the current in coil will decline. As a result, declination

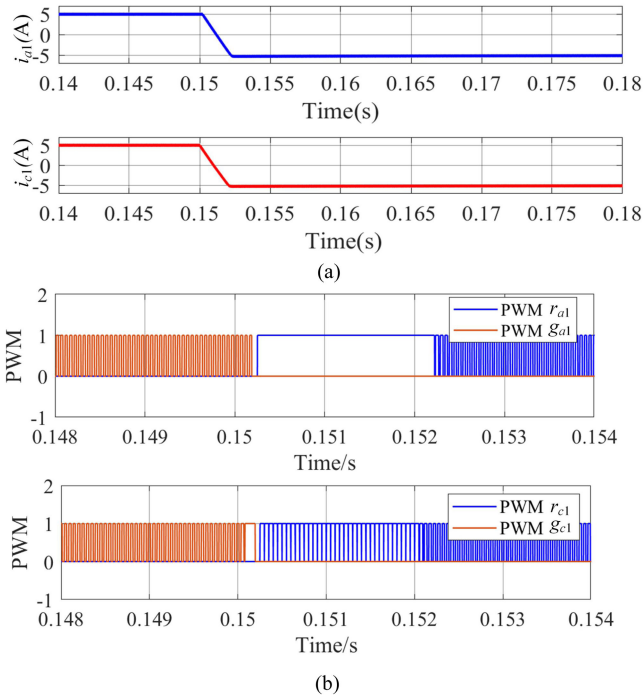

Fig. 15. Transition process of current reversing. (a) i_{a1} and i_{c1}. (b) PWM signals.

of current in certain coil can be applied for fault detection. However, when open-circuit fault occurs in one phase-leg, for example, i_{c1}, the rotor will deviate from the center. The position controller will react to this displacement so i_{a1} will also decline because of controller in this transient period. Declination caused by fault or control is hard to distinguish. The principle for fault detection and tolerant can be designed as: detecting $i_{a1}+ i_{c1}$, if there is no fault, $i_{a1}+ i_{c1}$ is supposed to equal to $2I_{\rm bias}$; if $i_{a1}+ i_{c1}$ decreases sharply, the fault can be judged as happened and switching the devices of i_{a1} and i_{c1}, to reverse the direction of current.

A simulation model is established to verify the proposed method. First, simulation of fault tolerant is carried on the amplifier, without position control. The current reference instructions of all coils are set as 5 A and a fault tolerant strategy is applied. At 0.15 s, open-circuit fault occurs in phase-leg of i_{c1}. The simulation results of i_{a1} and i_{c1} are shown in Fig. 15(a), PWM signals for switching devices are shown in Fig. 15(b). When the fault occurs, both i_{a1} and i_{c1} decline. According to PWM signals, spare switching devices are applied about four switching cycles after the fault occurs. The time span of the transient process of current reversing is about 3 ms.

Then, results of simulations for fault tolerant while rotating are shown in Fig. 16. The rotating speed is set as 4800 r/min. There is vibration in displacement because of centrifugal force. The device open-circuit fault occurs at 0.15 s, the reaction of displacement is shown in Fig. 16(a) and the current is shown in Fig. 16(b). The control current reverses within 5 ms. Because of the transient process in current, there is an overshoot in displacement, about 100 μm. Generally, the air gap of touch-down bearing is larger than 150 μm, so this overshoot cannot

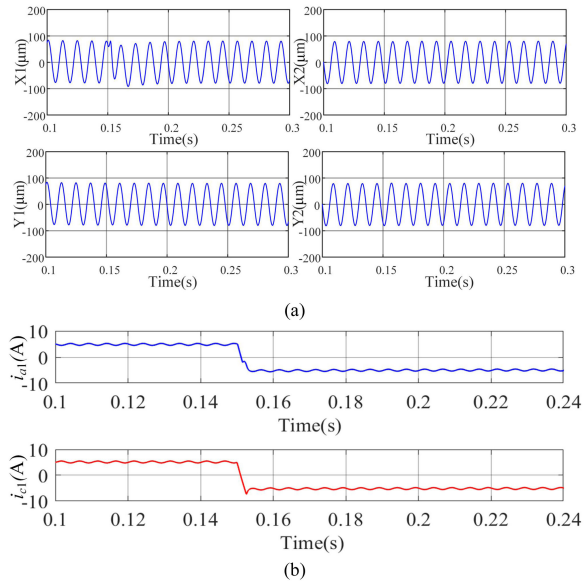

Fig. 16. Transition process of fault tolerant. (a) Position signals. (b) Current signals.

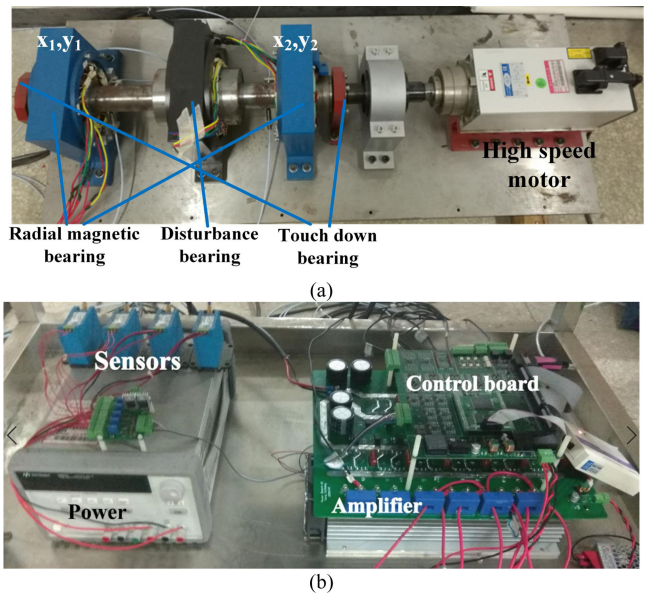

Fig. 17. Structure of AMB test rig. (a) Structure of magnetic bearing, (b) Physical figure of amplifier and control board.

cause friction and collision. The simulation shows that the AMB system can also work effectively while open-circuit occurs under the influence of fault tolerance strategy.

IV. Experiment Results

In order to verify the feasibility of the fault-tolerant strategy, the fault-tolerant control strategies have been verified on a four-axis AMB platform. The test rig includes two touchdown bearings, two radial AMBs, a shaft, and an HS motor etc. The structure of the test rig is shown in Fig. 17(a). The controller and amplifier are shown in Fig. 17(b). The main controller unit is digital signal processor (DSP) and switching device is chosen as

TABLE II
Major Parameters of the AMB System

Parameters	Values
Max electromagnetic force	1000N
Magnetic bearing air gap	500μm (total 1000μm)
Touch-down bearing air gap	250μm (total 500μm)
Shaft mass m	10kg
Magnetic bearing winding turns N	N 46/pole
Winding inductance L	10.8mH
Winding resistance R	0.5Ω
Force/displacement stiffness k_x	-2.6×10^6 N/m
Force/current stiffness k_i	260 N/A
DC bus voltage U_D	150V
Switching frequency f_s	20kHz
Bias current I_{bias}	5A
Max current I_{max}	10A

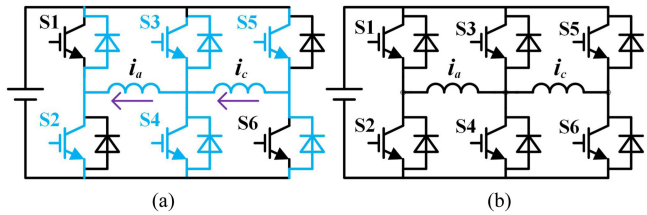

Fig. 18. Single degree of freedom normal working topology. (a) $X1$ axis for fault-tolerant control. (b) $Y1$ axis for normal operation.

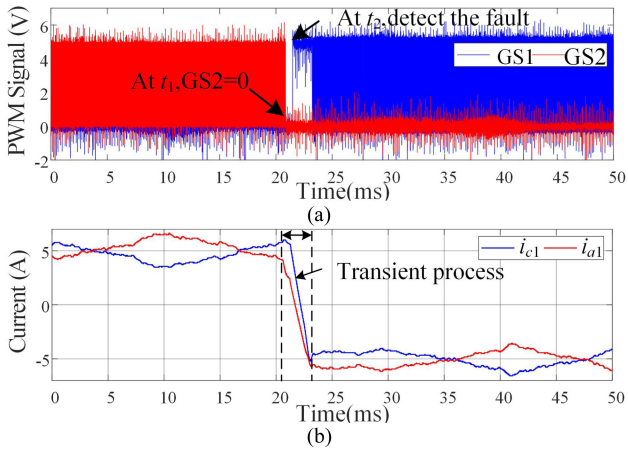

Fig. 19. Switching device $S2$ fault tolerance experiment results. (a) PWM signals of $S1$ and $S2$. (b) Transient process of the winding currents.

IGBT. When turning off a certain IGBT directly, an open-circuit error is emulated.

The basic experimental parameters and conditions are given in Table II.

A. Single Degree of Freedom Fault Tolerance Experiment

Taking the $X1$ axis as the degree of freedom of this fault-tolerant experiment, the $Y1$ axis and the $X1$ axis control the suspension of the front end of the magnetic bearing in the same plane. Under normal working conditions, the $X1$ axis adopts the working mode as shown in the figure, and the $Y1$ adopts the ordinary half-bridge structure, shown in Fig. 18.

As shown in Fig. 19. GS1 and GS2 are the PWM signals of the switching devices $S1$ and $S2$, respectively, and the rotation

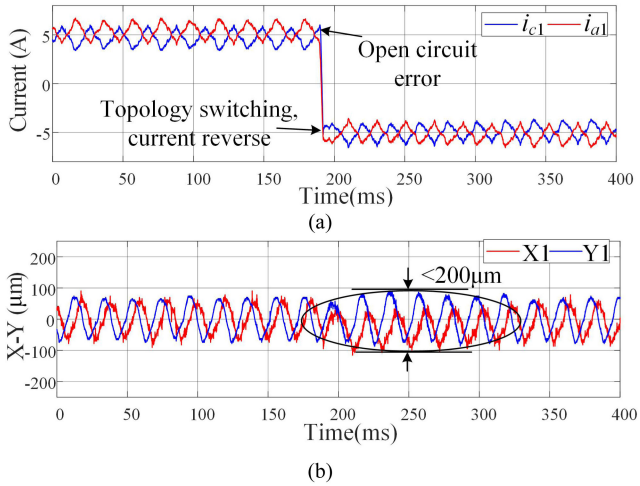

Fig. 20. Result of open-circuit fault occurs in switching device $S2$. (a) Current signals of i_{a1} and i_{c1}. (b) Position signals of $X1$ and $Y1$.

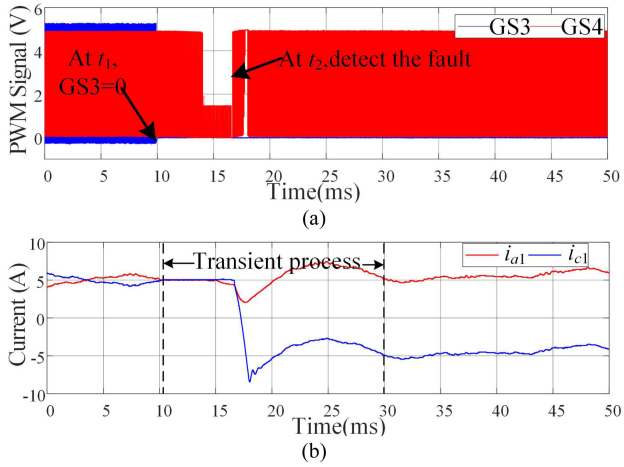

Fig. 21. Switching device $S3$ fault tolerance experiment results. (a) PWM signals of $S3$ and $S4$. (b) Transient process of the winding currents.

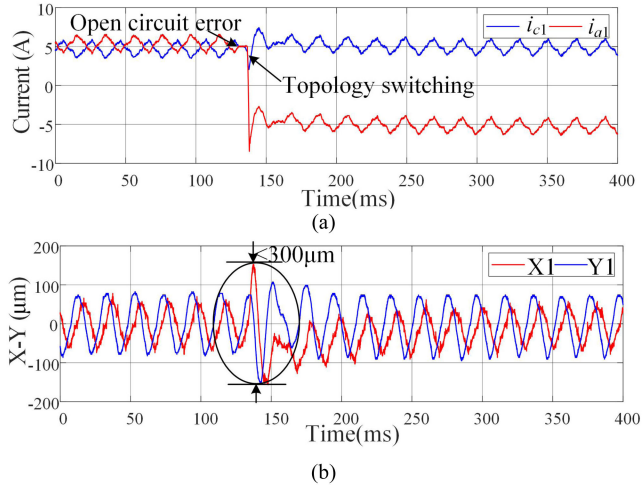

Fig. 22. Result of switching element $S3$ open-circuit fault. (a) Current signals of i_{a1} and i_{c1}. (b) Position signals of $X1$ and $Y1$.

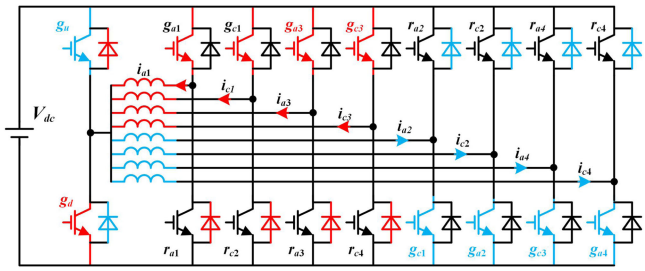

Fig. 23. Multiaxis fault-tolerant topology in experiments.

speed is set as 3000 r/min under normal working conditions. In the experiments, the corresponding IGBT is turned OFF to simulate the open-circuit fault. At t_1, $S2$ is turned off to emulate an open-circuit error of switching elements. It will take less than 2 ms to detect the fault and switch the topology at t_2, the two current directions are reversed at the same time, and the entire dynamic response time is less than 3 ms. The process from the occurrence of the failure to the restoration of stable operation does not exceed 5 ms. The fault tolerance principle of the switching device $S5$ is the same as $S2$, and the experimental phenomenon is similar to $S2$, so it is not explained here.

In the dynamic response process after the open-circuit fault of the switching device $S2$, due to topology switching, the current directions of the two windings are changed at the same time, the rotor displacement will also be affected and fluctuate. The fluctuation range of the rotor displacement is within ± 100 μm, which is much smaller than the protection gap, as shown in Fig. 20.

The result of the fault tolerance experiment of the switching device $S3$ is shown in Fig. 21. GS3 and GS4 are the PWM signals of the two switching devices of the middle bridge arm $S3$ and $S4$, respectively. Since the current will not change drastically after an open-circuit fault occurs in this case, the fault detection time is extended accordingly. A total of about 6 ms has elapsed from the occurrence of the failure to the detection of the failure. After the topology switches, the winding current i_{a1} reverses, and the system reaches a stable state again. The fault tolerance principle of the switching device $S4$ is the same as that of $S3$, and the experimental phenomenon is similar to that of $S3$, so it is not explained here.

Due to the slower fault detection speed, the rotor displacement fluctuation range is also slightly larger in this case, within ± 150 μm, but still within the protection gap 250 μm, which meets the fault tolerance requirements. In order to shorten the fault detection time, a smaller detection threshold can be selected according to the rotor rotation, shown in Fig. 22.

B. Multiaxis AMB Converter Fault Tolerance Experiment

The winding arrangement of the multiaxis fault-tolerant experiment is shown in Fig. 23. The $X1$ axis corresponds to the windings i_{a1} and i_{c1}, and the remaining three axes correspond to the remaining six windings.

In the experiment, the amplifier drives AMBs in normal mode to levitate the rotor under normal circumstances. The rotating speed is set at 4800 r/min. By turning off the switching device

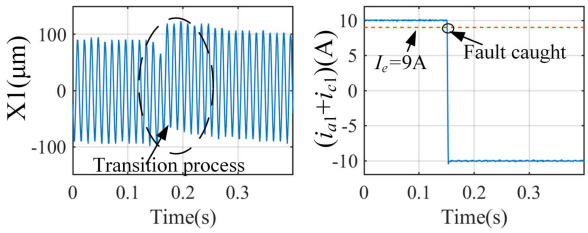

Fig. 24. Transition of displacement and fault detection.

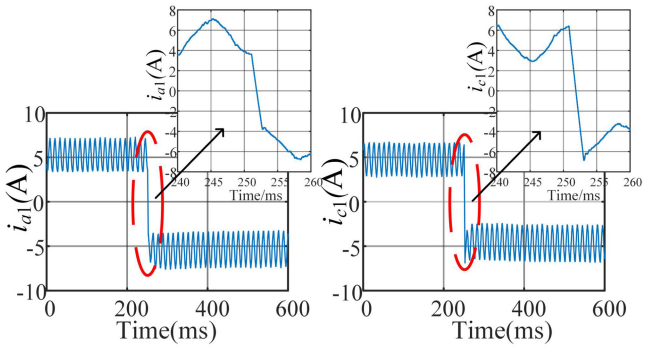

Fig. 25. Transition of current.

in phase-leg of i_{c1} artificially, an open-circuit fault can be emulated. The amplifier can detect the error automatically and reverse the current i_{a1} and i_{c1}. The displacement of $X1$ is shown in Fig. 24.

When the error occurs, the fault tolerant strategy is applied. The overshoot in the transition process is about 30 μm, after the transition process, the system is also stable. The process of fault detection is shown in Fig. 24.

Transition process of current is shown in Fig. 25, the time span of fault detection and current reversion is less than 30 ms. The corresponding current direction is reversed to keep suspension of the rotor.

V. Conclusion

From the perspective of improving the safety and reliability of AMB amplifiers, this article proposes open-circuit fault-tolerant control strategies for switching devices for different current control topologies.

For single-axis system, using a three-phase full-bridge topology to control the single-axis AMB with two windings current. There are four working modes. The fault can be detected within 5 ms after an open-circuit fault occurs in the switching device, and the fault device can be located. With the failure of any of the switching devices in normal mode, the converter can be quickly switched to the corresponding backup mode and keep the rotor with suspension. After expanding to a multiaxis system, it can still control the winding current of all degrees of freedom of the multiaxis magnetic bearing. It is divided into two working modes. After the switching device fails, the fault can be detected within 1 ms and the topology can be switched immediately. The proposed fault detection and control strategy improves the performance of the entire active magnetic levitation system with rotation.

References

[1] P. Dergachev, A. Kosterin, E. Kurbatova, and P. Kurbatov, "Flywheel energy storage system with magnetic HTS suspension and embedded in the flywheel motor-generator," in *Proc. IEEE Int. Power Electron. Motion Control Conf*., 2016, pp. 574–579.

[2] A. Smirnov, N. Uzhegov, T. Sillanpää, J. Pyrhönen, and O. Pyrhönen, "High-speed electrical machine with active magnetic bearing system optimization," *IEEE Trans. Ind. Electron.*, vol. 64, no. 12, pp. 9876–9885, Dec. 2017.

[3] N. Kurita, T. Ishikawa, N. Saito, T. Masuzawa, and D. Timms, "A double-sided stator type axial self-bearing motor development for total artificial heart," in *Proc. IEEE Int. Elect. Mach. Drives Conf.*, 2017, pp. 1–6.

[4] J. Denk, D. Stoiber, H. Kopken, and H. Walter, "Industrialization of AMB systems with standard drive technology," *IEEE Trans. Ind. Appl.*, vol. 49, no. 2, pp. 791–798, Mar./Apr. 2013.

[5] G. Schweitzer, E. H. Maslen, H. Bleuler, and M. Cole, *Magnetic Bearings: Theory, Design, and Application to Rotating Machinery*. Berlin, Germany: Springer, 2010.

[6] J. Yu and C. Zhu, "A sensor-fault tolerant control method of active magnetic bearing in flywheel energy storage system," in *Proc. IEEE Veh. Power Propulsion Conf.*, 2016, pp. 1–6.

[7] F. M. Flinders, P. J. Wolfs, and K. C. Kwong, "Improved techniques for switching power amplifiers," *IEEE Trans. Power Electron.*, vol. 8, no. 4, pp. 673–679, Oct. 1993.

[8] H. Ertl, J. W. Kolar, and F. C. Zach, "Basic considerations and topologies of switched-mode assisted linear power amplifiers," *IEEE Trans. Ind. Electron.*, vol. 44, no. 1, pp. 116–123, Feb. 1997.

[9] C. Wei and D. Söffker, "Optimization strategy for PID-controller design of AMB rotor systems," *IEEE Trans. Control Syst. Technol.*, vol. 24, no. 3, pp. 788–803, May 2016.

[10] H. Sun, D. Jiang, J. Ding, and J. Yang, "Multifrequency vibration suppression of magnetic bearing systems applied variable step-size automatic learning control," in *Proc. IEEE Energy Convers. Congr. Expo.*, 2020, pp. 3193–3198.

[11] S. Wang, H. Zhu, M. Wu, and W. Zhang, "Active disturbance rejection decoupling control for three-degree-of-freedom six-pole active magnetic bearing based on BP neural network," *IEEE Trans. Appl. Supercond.*, vol. 30, no. 4, Jun. 2020, Art no. 3603505.

[12] Y. He, X. He, J. Ma, and Y. Fang, "Optimization research on a switching power amplifier and a current control strategy of active magnetic bearing," *IEEE Access*, vol. 8, pp. 34833–34841, 2020.

[13] A. Noshadi, J. Shi, W. S. Lee, P. Shi, and A. Kalam, "System identification and robust control of multi-input multi-output active magnetic bearing systems," *IEEE Trans. Control Syst. Technol.*, vol. 24, no. 4, pp. 1227–1239, Jul. 2016.

[14] D. Jiang and P. Kshirsagar, "Analysis and control of a novel power electronics converter for active magnetic bearing drive," *IEEE Trans. Ind. Appl.*, vol. 53, no. 3, pp. 2222–2232, May/Jun. 2017.

[15] D. Jiang, T. Li, Z. Hu, and H. Sun, "Novel topologies of power electronics converter as active magnetic bearing drive," *IEEE Trans. Ind. Electron.*, vol. 67, no. 2, pp. 950–959, Feb. 2020.

[16] X. Cheng, S. Deng, B. -X. Cheng, Y. -F. Hu, H. -C. Wu, and R.-G. Zhou, "Design and implementation of a fault-tolerant magnetic bearing control system combined with a novel fault-diagnosis of actuators," *IEEE Access*, vol. 9, pp. 2454–2465, 2021.

[17] J. Yang, D. Jiang, H. Sun, J. Ding, A. Li, and Z. Liu, "A Series-winding topology converter with capability of fault-tolerant operation for active magnetic bearing drive," *IEEE Trans. Ind. Electron.*, vol. 69, no. 7, pp. 6678–6687, Jul. 2022.

[18] H.-S. Ro, D.-H. Kim, H.-G. Jeong, and K.-B. Lee, "Tolerant control for power transistor faults in switched reluctance motor drives," *IEEE Trans. Ind. Appl.*, vol. 51, no. 4, pp. 3187–3197, Jul./Aug. 2015.

[19] U. Choi, J. Lee, F. Blaabjerg, and K. Lee, "Open-circuit fault diagnosis and fault-tolerant control for a grid-connected NPC inverter," *IEEE Trans. Power Electron.*, vol. 31, no. 10, pp. 7234–7247, Oct. 2016.

[20] H. Guo, J. Xu, and Y. Chen, "Robust control of fault-tolerant permanent-magnet synchronous motor for aerospace application with guaranteed fault switch process," *IEEE Trans. Ind. Electron.*, vol. 62, no. 12, pp. 7309–7321, Dec. 2015.
[21] S. Yang, Y. Tang, and P. Wang, "Seamless fault-tolerant operation of a modular multilevel converter with switch open-circuit fault diagnosis in a distributed control architecture," *IEEE Trans. Power Electron.*, vol. 33, no. 8, pp. 7058–7070, Aug. 2018.
[22] T. Zhang and Q. Le, "Research on the fault tolerance performances of the nine-pole radial hybrid magnetic bearing," in *Proc. IEEE Int. Conf. Appl. Supercond. Electromagn. Devices*, 2020, pp. 1–2.
[23] Z. Fu, D. Jiang, and R. Qu, "Design of four-axis magnetic bearing for high speed motor," in *Proc. IEEE Int. Power Electron. Motion Control Conf.*, 2016, pp. 786–791, doi: 10.1109/IPEMC.2016.7512385.

Jianfu Ding (Student Member, IEEE) was born in Liaoning, China, in 1998. He received the B.S. degree in electrical engineering in 2020 from Huazhong University of Science and Technology, Wuhan, China, where he is currently working toward the M.S. degree with China-EU Institute for Clean and Renewable Energy.

His current research focuses on fault-tolerant converter topology, control strategy and identification of eccentricity of rotor for active magnetic bearing.

Hongbo Sun was born in Shandong, China, in 1995. He received the B.S. degree in hydraulic engineering and the M.S. degree in electrical engineering, from Huazhong University of Science and Technology, Wuhan, China, in 2018 and 2020, respectively.

He is currently an Engineer with China Ship Development and Design Center, Wuhan, China. His current research focuses on vibration suppression for active magnetic bearing.

Dong Jiang (Senior Member, IEEE) received the B.S. and M.S. degrees in electrical engineering from Tsinghua University, Beijing, China, in 2005 and 2007, respectively, and the Ph.D. degree in power electronics and motor drives from the University of Tennessee, Knoxville, TN, USA, in 2011.

He was with the United Technologies Research Center, East Hartford, CT, USA, as a Senior Research Scientist/Engineer, from January 2012 to July 2015. He has been with the Huazhong University of Science and Technology, Wuhan, China, as a Professor, since July 2015. His main research interests include power electronics and motor drives, with more than 100 published IEEE journal and conference papers in this area.

Dr. Jiang was the recipient of six best paper awards in IEEE conferences. He is currently an Associate Editor for the IEEE TRANSACTIONS ON INDUSTRY APPLICATIONS and the Chair of the IEEE Power Electronics Society Wuhan Chapter.

Jichang Yang was born in Hunan, China, in 1997. He received the B.S. degree in electrical engineering in 2019 from Huazhong University of Science and Technology, Wuhan, China, where he is currently working toward the M.S. degree with the School of Electronic and Electrical Engineering.

His current research focuses on converter topology, control strategy and self-sensing method for active magnetic bearing.

Zicheng Liu (Member, IEEE) was born in Shandong, China, in 1989. He received the B.S. degree in hydropower engineering from Huazhong University of Science and Technology (HUST), Wuhan, China, in 2011, and the Ph.D. degree in electrical engineering from Tsinghua University, Beijing, China, in 2016.

From October 2014 to March 2015, he was a Visiting Student with Purdue University, West Lafayette, IN, USA. From June 2016 to September 2018, he was a Postdoctoral Researcher with Beijing Jiaotong University, Beijing, China. He is currently an Associate Professor with HUST. His research interests include multiphase motor control systems and transportation electrification.